

PHYSICAL REVIEW LETTERS

VOLUME 24

23 FEBRUARY 1970

NUMBER 8

COLLISION SPECTROSCOPY OF THE SYSTEM Li_2^+*

W. Aberth, O. Bernardini,[†] D. Coffey, Jr.,[‡] D. C. Lorents, and R. E. Olson
Stanford Research Institute, Menlo Park, California 94025

(Received 19 January 1970)

Differential scattering measurements are reported for the elastic reaction $\text{Li}^+ + \text{Li} \rightarrow \text{Li}^+ + \text{Li}$ at 25–150 eV (c.m.) and the inelastic reaction $\text{Li}^+ + \text{Li}(2s^2S) \rightarrow \text{Li}^+ + \text{Li}(2p^2P)$ at 25, 50, and 100 eV. The elastic cross sections show a rainbow peak at $E\theta_R \cong 80$ eV deg, curve-crossing perturbations, and possibly electron-transfer oscillations. The inelastic cross sections have an oscillatory structure with a threshold at $E\theta_x \cong 70$ eV deg. These observations are interpreted in terms of the diabatic electronic states of Li_2^+ .

Differential cross-section measurements of low-energy elastic and inelastic ion-atom scattering for few-electron systems have proven particularly fruitful for observing various interactions and for comparing with the predictions of theoretical models.¹ The electron- and nuclear-exchange interactions of the $\text{He}^+ + \text{He}$ system have been observed and studied in great detail.² The role of diabatic states for that system, and their intimate relationship to curve-crossing interactions, are currently being intensively investigated both theoretically and experimentally.³ The next simplest symmetric system, $\text{Li}^+ + \text{Li}$, has been considered qualitatively by Lichten,⁴ who concluded that, due to the small separation of the Σ_g and Σ_u diabatic states arising from the ground-state separated atoms, the electron-transfer oscillations seen in the differential cross sections would be of long wavelength and heavily damped. The total charge-exchange cross section has been measured as a function of energy.⁵ Its magnitude and structure are consistent with a difference potential $\Delta V_{ad}(R)$ from an adiabatic computation^{5b} of the Σ_g and Σ_u states of Li_2^+ , the oscillations being due to an extremum in ΔV at about 5 a.u. Such measurements do not test the difference potential very thoroughly,

since oscillations in the total cross section are sensitive to changes in ΔV only near the extremum and outside it.⁶ In this paper we present the first results of a study of elastic and inelastic differential scattering in $\text{Li}^+ + \text{Li}$, which allows one to deduce much more information on the potentials.

The apparatus⁷ used earlier for measurements of Li^+ scattering by He was modified for these measurements by installation of a Li-vapor beam source to replace the gas scattering cell. Isotopically pure $^7\text{Li}^+$ ions obtained from an indirectly heated spodumene source were accelerated and focused using an ion gun described previously.⁸ A collimated ion beam intersected a beam of ^7Li atoms directed perpendicular to the plane of rotation of the scattered ion detector and containing the ion beam. The scattered ion beam defined by a pair of slits was electrostatically energy analyzed and detected with an electron multiplier. The slit sizes were unchanged from those used in the previous experiment,⁷ the effective angular resolution being about 0.2° for angles greater than 5° . Before energy analysis, the scattered ions were retarded to 50 eV to improve the resolution of the analyzer. The energy resolution was always sufficient to assure com-

plete isolation of the elastic peak as well as the peak due to the excitation of $\text{Li}(2p)$.

The unnormalized cross sections σ are presented in Figs. 1 and 2 as reduced cross sections $\rho = \theta \sin\theta\sigma(\theta, E)$ versus the reduced angle $\tau = E\theta$. For scattering at small and moderate angles,⁹ these both depend primarily on the impact parameter b : $\tau = \tau(b)$ and $\rho = \rho(\tau)$.

Although we have not yet measured absolute cross sections, it was possible to obtain the ratio of the signals in the $2p$ and the elastic channel at each angle θ at $E = 25, 50,$ and 100 eV. These ratios oscillate as a function of τ with an envelope that rises sharply with increasing τ to a peak and falls off more gradually. The three envelopes are similar in shape but the 50-eV en-

velope lies above the other two for all values of τ .

Various noteworthy features can be seen in the elastic curves (Fig. 1). A rainbow peak is identified at $\tau_R = 80$ eV deg. A localized high-frequency oscillation at $\tau_x^{\text{el}} = 250$ eV deg is attributed to a perturbation due to a curve crossing like those seen in other systems¹⁰; its amplitude is greatest at about 40 eV. The electron-transfer oscillations are expected to have low frequencies and small amplitudes,⁴ and to be unlocalized; they may be present, but they are difficult to identify in the presence of the prominent

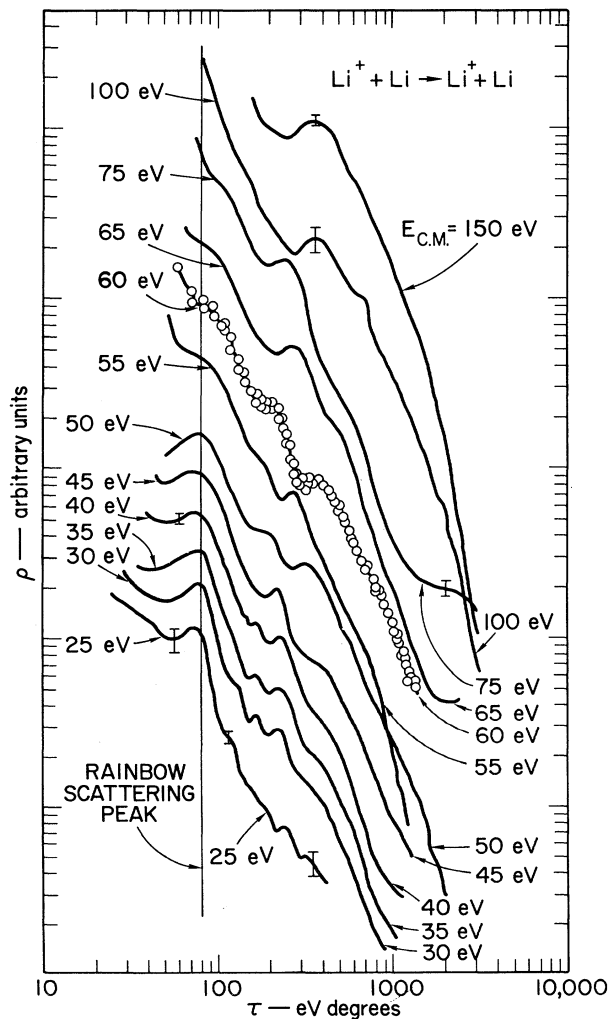


FIG. 1. Elastic data in units of $\rho = \theta \sin\theta\sigma(\theta)$ vs $\tau = E\theta$. The error bars indicate the limits of reproducibility of the data over two or more data runs. The 60-eV curve shows the data points from two runs.

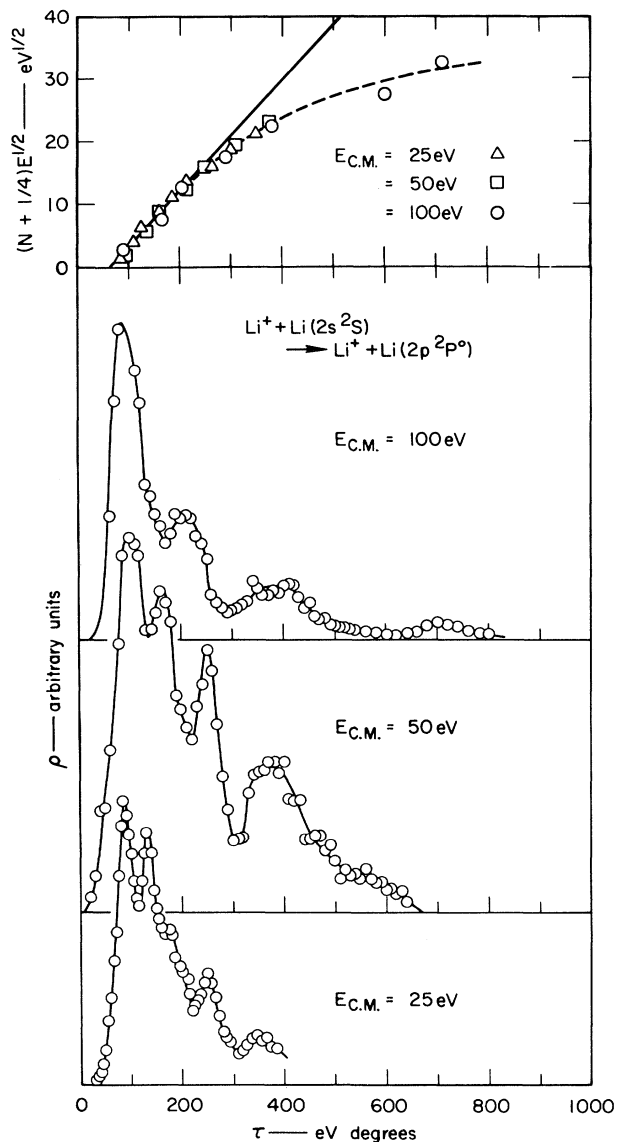


FIG. 2. Lower: Inelastic data in the reduced units of τ and ρ . Upper: Reduced plot of peak and valley indices for the inelastic data.

local features.

The excitation data (Fig. 2) exhibit a sharp onset at a remarkably low value of $\tau_x^{\text{inel}} = 70$ eV deg. The oscillations following the onset are not large and rapidly decay with increasing τ .

To explain these results we have constructed an approximate potential diagram in Fig. 3, using the known separated-atom and united-atom limits for the various states and a recent calculation by Fischer and Kemmey¹¹ (FK) of the lowest adiabatic Σ_g and Σ_u states for $4 \leq R \leq 8$ a.u. All solid curves are diabatic, as defined by Lichten,^{4,12} and thus even with the same symmetry they may cross one another.

The key to the explanation of the elastic perturbation and inelastic effects is the $F\Sigma_u$ state, which provides a strong coupling mechanism between the $A\Sigma_u$ and $C\Sigma_u, E\Sigma_u$, and higher states. The $F\Sigma_u$ state with the configuration $(1s\sigma_g)^2 \times (1s\sigma_u)(2s\sigma_g)^2$ correlates at $R=0$ with the ground state of the united atom $C^+(1s^2 2s^2 2p)$, and at $R=\infty$ with the highly excited separated-atom state $\text{Li}^+(1s^2) + \text{Li}(1s 2s^2)$, which probably lies at an energy of about 2 a.u. The ground $X\Sigma_g$ state correlates at $R=0$ with the excited state $C^+(1s^2 2s 2p^2)$, and so must cross the F state, while the $A\Sigma_u$ and $C\Sigma_u$ states correlate, respectively, with the $1s^2 2p^2 3p$ and $1s^2 2p^2 4f$ configurations of C^+ . The ground adiabatic Σ_u state corresponds to our A state for $R > R_x$ where R_x is the F - A crossing point. The F state and its crossings with A and X explain both the maximum and the change in sign observed in the adiabatic ground-state difference potential ΔV_{ad} , as calculated by Peek, Green, Perel, and Michels^{5b} (PGPM). Their adiabatic Σ_u - Σ_g crossover at $R=3.0$ a.u. locates the crossing of the F and X states in Fig. 3. Although ΔV_{ad} differs signifi-

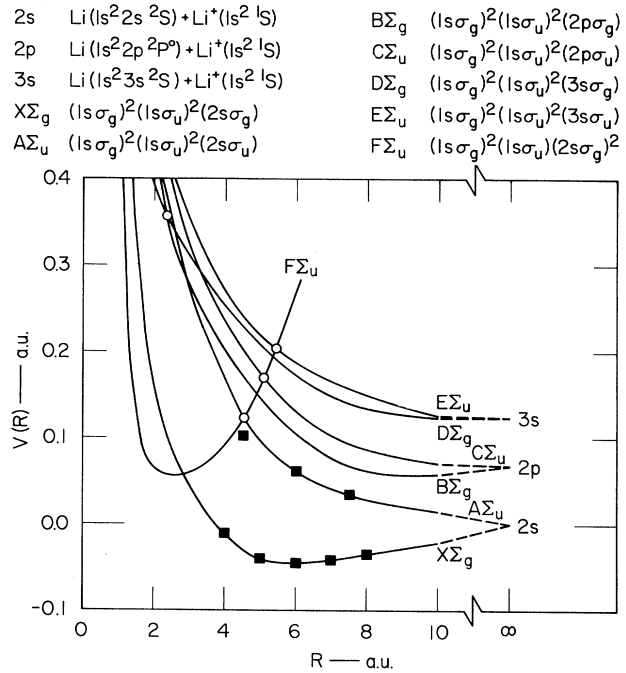


FIG. 3. The diabatic potential curves for the Li_2^+ system. The FK calculations are shown by the solid squares and the crossing points by the open circles. The curves are estimates of the potentials based upon the FK and PGPM calculations, the united- and separated-atom limits of the various states, and the scattering data. The X, A, B, C, \dots lettering scheme is arbitrary.

cantly as calculated by PGPM and by FK, both versions reproduce the experimental total cross sections equally well.

We have based our X - and A -state potentials in Fig. 3 on the calculations of FK, extending the former to small R by using a shell-model Bohr (shielded Coulomb) potential with simple hydrogenic shielding coefficients¹³:

$$\begin{aligned}
 V_X(R) &= R^{-1} [1 + 2 \exp(-2.36R)] [\exp(-0.63R) + 2 \exp(-2.36R)] \quad (R < 3.5 \text{ a.u.}); \\
 &= 0.0456 \{ \exp[4.18(1-R/5.7)] - 2 \exp[2.09(1-R/5.7)] \} \quad (3.5 < R < 5.7); \\
 &= 0.0456 \{ \exp[3.26(1-R/5.7)] - 2 \exp[1.63(1-R/5.7)] \} \quad (5.7 < R).
 \end{aligned} \tag{1}$$

The second and third forms are Morse functions with a broad minimum at $R_m = 5.7$ a.u. with a depth $\epsilon = 0.0456$ a.u. From this potential the calculated reduced rainbow angle τ_R is 84.3 eV deg at high energy, and 75 eV deg at 15 eV, agreeing with the experimental value $\tau_R = 80$ eV deg. The X and A potentials are related by the difference potential (in atomic units)

$$V_A(R) - V_X(R) = \Delta V(R) = 0.50 \exp(-0.26R), \tag{2}$$

which is obtained from a semilog plot of FK's data; it extrapolates at $R=0$ to 0.5 a.u. in agreement with Lichten.⁴ The perturbation at $\tau_x = 250$ eV deg was used in conjunction with the deflection function for V_A to locate the F - A crossing at $R_x = 4.5$ a.u.

The oscillations on both the elastic and inelastic differential cross sections due to the $A\Sigma_u - F\Sigma_u$ interaction are explained by the Stueckelberg theory of curve crossing. Transitions occur only at or near a crossing point R_x where the electronic states are degenerate, and this point is passed twice in the collision. Two opportunities for transition result in two possible trajectories for both elastic and inelastic scattering at a given angle θ , giving rise to quantal interference oscillations on both the elastic and inelastic differential cross sections. The frequency of these oscillations is related to the difference in impact parameters for scattering to the angle θ by

$$\Delta b = 2\pi\hbar(2\mu E)^{-1/2}(dN/d\theta), \quad (3)$$

where N is an integer index for the peaks. An appropriate reduced plot that takes into account threshold effects and the expected energy dependence presents $(N + \frac{1}{4})E^{1/2}$ vs τ ; its slope is proportional to Δb . In the upper portion of Fig. 2, the inelastic oscillations have been so plotted. The zero intercept yields the threshold value of $\tau_x^{\text{inel}} = 70$ eV deg for this process, and the initial slope gives $\Delta b^{\text{inel}} = 1.5$ a.u., a large value which implies that the A and F potentials are well separated for $R < R_x$. Likewise, the spacing in the elastic oscillating perturbation at $\tau^{\text{el}} = 250$ eV deg yields $\Delta b^{\text{el}} = 1.8$ a.u. The fact that Δb^{el} is slightly larger than Δb^{inel} is in accord with theory. Semiclassically the thresholds are related by

$$\tau_x^{\text{inel}} = (\tau_x^{\text{el}} + \tau_x^{\text{CF}})/2, \quad (4)$$

where τ_x^{CF} is the reduced angle for elastic scattering following the C -state potential outside the CF crossing and the F state inside, and with just the proper impact parameter to reach R_x , the FA crossing. We thus find $\tau_x^{\text{CF}} = -110$ eV deg; this negative scattering angle presumably arises from the strongly attractive F -state potential in the region between R_x and the CF crossing.

The magnitude of the coupling matrix element $H_{AF}(R_x)$ between the A and F states (half the adiabatic splitting) at this point can be estimated from the energy 40 eV at which the elastic perturbation has maximum amplitude (confirmed by the maximum in the inelastic transition probability near 50 eV). Using the Landau-Zener formula together with an estimate of the slopes of the F and A potentials near R_x , we obtain an upper bound (because the centrifugal contribution is unknown), $H_{AF}(R_x) < 0.018$ a.u. At energies

much higher than 40 eV the particles will predominantly follow the $A\Sigma_u$ curve through R_x and remain on the diabatic potential.

The results presented here give an approximate picture of the diabatic states of Li_2^+ consistent with the available experimental data and molecular-state computations. For further study of this interesting system it is of utmost importance that more *ab initio* computations of the ground and excited electronic states be carried out. Experimental studies are continuing in this laboratory to establish the absolute cross sections and to observe excitation of the $\text{Li}(3s)$ and higher states.

The authors wish to thank Dr. C. R. Fischer and Dr. P. J. Kemmey for a preprint of the Li_2^+ potential calculations as well as Dr. J. R. Sheridan for assistance in data taking. We express our sincere appreciation to our colleague, Dr. F. T. Smith, for many helpful discussions and for assistance with the manuscript.

*The experimental work was supported in part by the U. S. Army Research Office (Durham). The theoretical interpretation was supported by the Atomic Energy Commission.

†Present address: Ente Nazionale Idrocarburi, Milan, Italy.

‡Present address: Department of Chemistry, San Diego State College, San Diego, Calif.

¹For example: F. T. Smith, in *Lectures in Theoretical Physics: Atomic Collision Processes*, edited by S. Geltman, K. T. Mahanthappa, and W. E. Brittin (Gordon and Breach, New York, 1969), Vol. XIC, p. 95.

²F. P. Ziemba and E. Everhart, *Phys. Rev. Letters* **2**, 299 (1959); G. J. Lockwood, H. F. Helbig, and E. Everhart, *Phys. Rev.* **132**, 3078 (1963); D. C. Lorents and W. Aberth, *Phys. Rev.* **139**, A1017 (1965); W. Aberth, D. C. Lorents, R. P. Marchi, and F. T. Smith, *Phys. Rev. Letters* **15**, 742 (1965); J. Baudon, M. Abignoli, M. Barat, and A. Pernot, *Phys. Letters* **25A**, 564 (1967).

³D. C. Lorents, W. Aberth, and V. W. Hesterman, *Phys. Rev. Letters* **17**, 849 (1966); R. P. Marchi and F. T. Smith, *Phys. Rev.* **139**, A1025 (1965); M. Kennedy and F. J. Smith, *Mol. Phys.* **16**, 131 (1969); R. P. Marchi, *Phys. Rev.* **183**, 185 (1969).

⁴W. Lichten, *Phys. Rev.* **131**, 229 (1963).

^{5a}D. C. Lorents, G. Black, and O. Heinz, *Phys. Rev.* **137**, A1049 (1965).

^{5b}J. M. Peek, T. A. Green, J. Perel, and H. H. Michels, *Phys. Rev. Letters* **20**, 1419 (1968).

^{5c}J. Perel, H. L. Daley, J. M. Peek, and T. A. Green, *Phys. Rev. Letters* **23**, 677 (1969).

⁶R. E. Olson, *Phys. Rev.* (to be published).

⁷W. Aberth and D. C. Lorents, *Phys. Rev.* **182**, 162 (1969).

⁸H. Haskell, O. Heinz, and D. C. Lorents, *Rev. Sci.*

Instr. 37, 607 (1966).

⁹F. T. Smith, R. P. Marchi, and K. G. Dedrick, Phys. Rev. 150, 79 (1966).

¹⁰F. T. Smith, D. C. Lorents, W. Aberth, and R. P. Marchi, Phys. Rev. Letters 15, 742 (1965).

¹¹C. R. Fischer and P. J. Kemmey, Phys. Rev. 186, 272 (1969).

¹²W. Lichten, Phys. Rev. 164, 131 (1967).

¹³F. T. Smith, R. P. Marchi, W. Aberth, D. C. Lorents, and O. Heinz, Phys. Rev. 161, 31 (1967).

SURFACE EFFECTS ON POSITRON ANNIHILATION IN SILICON POWDERS*

A. Gainotti and C. Ghezzi

Istituto di Fisica dell'Università, Parma, Italy

(Received 29 October 1969)

Positron lifetime measurements were made in silicon powder samples with different grain size and doping. Two lifetime components were detected in low-resistivity *n* samples and in high-resistivity *p* samples having grain sizes smaller than about 50 μ . The faster component [$\tau_1 = (2.59 \pm 0.10) \times 10^{-10}$ sec] was easily ascribed to annihilations in the bulk; the slower one [$\tau_2 = (5.20 \pm 0.20) \times 10^{-10}$ sec] was ascribed to annihilation processes taking place in the oxide surface layer.

Positron-lifetime spectra in silicon single crystals have been extensively studied by several workers¹⁻⁴ and are commonly interpreted in terms of a single significant decay component τ_1 which appears to be independent of the type and the amount of doping. The lifetime τ_1 was found to depend strongly on the mean valence-electron density and the polarizability of the valence band, and was then ascribed to annihilations with the electrons of the valence band.⁴ In this paper we report positron-lifetime measurements in silicon powder samples where a slower decay component τ_2 is also observed. The experimental data suggest that this new component τ_2 is due to annihilation processes which take place near the surfaces of the grains.

The experimental technique for the recording and analysis of the lifetime spectra has been described previously.⁴ With narrow energy-selection windows set near the Compton edges of the Na²² spectrum, the full width at half-maximum (FWHM) of the prompt time-resolution curve taken with the γ rays emitted by Co⁶⁰ was 3.5×10^{-10} sec. The peak-to-background ratio was 10⁴:1.

First we measured the positron lifetime in a single-crystal sample. The same single crystal was then powdered in atmospheric air in order to obtain several powder samples of different grain sizes. The mean diameter of the powder grains was measured by means of an optical microscope, and finally positron-lifetime spectra of each sample were taken. In order to avoid the presence of dust and humidity, all lifetime measurements were taken in a vacuum (10^{-4} Torr). The whole process was carried out for (a) *n*-type

samples with 2×10^{18} Sb atoms/cm³, (b) *p*-type samples with 3×10^{18} B atoms/cm³, and (c) *p*-type samples with 8×10^{14} B atoms/cm³. In all three cases we started with single-crystal samples where only one significant lifetime $\tau_1 = (2.62 \pm 0.015) \times 10^{-10}$ sec was detected; a second tail component was also present with a maximum intensity of 2.7% and a lifetime ranging from 5.3×10^{-10} to 14.8×10^{-10} sec. This latter component may be ascribed to spurious effects as was explained in previous works.^{3,4}

In powder samples we found identical results as for single crystals when we examined samples having grain size greater than about 50 μ . Then, in case (a) the abrupt appearance of a slower decay component τ_2 [with lifetime $\tau_2 = (5.20 \pm 0.20) \times 10^{-10}$ sec] was observed. Subsequently the intensity I_2 of the new component showed a slow increase with decreasing grain size up to 25% for grain sizes of about 2-3 μ .

In Fig. 1 a typical decay spectrum is reported where the slower component is clearly evidenced. The effect is considerably less marked in case (b), and no one significant τ_2 component was observed in low-resistivity *p*-type samples [case (c)]. Finally, it must be pointed out that the τ_1 fast component was always detected in all powder samples with an averaged lifetime [$\tau_1 = (2.59 \pm 0.10) \times 10^{-10}$ sec] which is, significantly, equal to the single-crystal lifetime and can therefore be ascribed to the same annihilation process which was assumed for single crystals.

The first suggestion is that the slow component is due to positrons which annihilate near the grain surfaces, being captured by a surface potential well. Then, following Brandt and Paulin,⁵